

SPT Based Liquefaction Hazard Assessments in Iğdır City (Türkiye)

Yusuf Güzel *¹, Muhammed Alperen Özdemir²

*¹ Necmettin Erbakan University, Faculty of Engineering and Architecture, Civil Engineering, KONYA
² Iğdır University, Faculty of Agriculture, Civil Engineering, IĞDIR

(Alınış / Received: 23.01.2024, Kabul / Accepted: 31.03.2024, Online Yayınlanma / Published Online: 30.04.2024)

Keywords

Seismic intensity level,
Standard penetration test,
Liquefaction potential index,
Liquefaction severity index,
Liquefaction potential
mapping

Abstract: Seismically active regions are always prone to be subjected to earthquake events and their eventual damages to urban areas. Liquefaction is one of the earthquake related incidents occurring within soil bodies during or after earthquake excitations. Gaining the knowledge of liquefaction potential for a site is exceedingly crucial in view of seismic risk mitigation, earthquake hazard assessments and future planning of urban areas. This study evaluates the liquefaction potential of Iğdır city located in the eastern-side of Türkiye, having borderlines with three other seismically active countries in the region, Armenia, Nakhichevan and Iran. Soil data (i.e., Standard Penetration Test values, water table, water content, unit weight, grain size distribution and Atterberg limits) at the considered areas within the city is gathered from 85 boreholes. After investigating the fault lines around the city, the two possible maximum peak ground accelerations involved in this study are determined to be 0.393g and 0.225g. Liquefaction susceptibility maps of the areas at the two peak ground acceleration levels are designated in regard to liquefaction potential index and liquefaction severity index methods. The studied areas in the city exhibit various levels of liquefaction susceptibility as the severity is observed to be greater under the larger peak ground acceleration.

Iğdır İlinde Sıvılaşma Tehlikesi Değerlendirmesi (Türkiye)

Anahtar Kelimeler

Sismik şiddet seviyesi,
Standard Penetrasyon
deneyi,
Sıvılaşma potansiyel
indeksi,
Sıvılaşma şiddet indeksi,
Sıvılaşma potansiyel
haritası

Öz: Sismik olarak aktif bölgeler her zaman deprem olaylarına ve bunların kentsel alanlara nihai zararlarına maruz kalmaya eğilimlidir. Sıvılaşma, deprem uyarımları sırasında veya sonrasında zemin içerisinde meydana gelen olaylardan biridir. Bir sahanın sıvılaşma potansiyeli hakkında bilgi edinmek, sismik riskin azaltılması, deprem tehlikesi değerlendirmeleri ve kentsel alanların gelecekteki planlaması açısından son derece önemlidir. Bu çalışma, Türkiye'nin doğusunda yer alan ve bölgedeki diğer üç sismik olarak aktif ülke olan Ermenistan, Nahçıvan ve İran ile sınırı bulunan Iğdır şehrinin sıvılaşma potansiyelini değerlendirmektedir. Şehir içinde ele alınan alanlardaki zemin verileri (Standart Penetrasyon Testi değerleri, su tablası, su içeriği, birim hacim ağırlık, tane boyutu dağılımı ve Atterberg limitleri) 85 sondaj kuyusundan toplanmıştır. Şehir çevresindeki fay hatları incelendikten sonra, bu çalışmada yer alan iki olası maksimum yer ivmesi 0.393g ve 0.225g olarak belirlenmiştir. En büyük iki yer ivmeleri altında çalışma sahalarının sıvılaşma duyarlılık haritaları, sıvılaşma potansiyel indeksi ve sıvılaşma şiddet indeksi yöntemlerine göre belirlenmiştir. Şehirde incelenen alanlar, maksimum yer ivmesi altında şiddetin daha fazla olduğu gözlemlendiğinden, çeşitli seviyelerde sıvılaşma duyarlılığı sergilemektedir.

*İlgili Yazar, email: yusufkurtdereli@hotmail.com

1. Introduction

Liquefaction is known as one of the earthquake triggered phenomena attributed to stress and stiffness losses due to increase of pore water pressure within saturated granular soil bodies. When soil layers no longer possess enough strength characteristics during earthquake excitations, the soil behaves as a viscous liquid [1]. This makes the ground surface structures to endure, to some extent, varied types of damages that burden great level of economic costs and, probably and most importantly, human casualties. Slope failures, earth dam failures, building and bridge foundation failures and damages to the pavement and buried infrastructures (i.e. gas, electric, and water pipelines) are the main consequences of liquefaction phenomenon [2]. Such types of damages were observed early in 1964 during and after the Good Friday earthquake in Alaska and the Niigata earthquake in Japan [3]. Moreover, relatively recently occurred the Duzce earthquake in 1999 [4], the Christchurch earthquake in 2010 [5], the Emilia earthquake in 2012 [6], the Japan earthquake in 2011 [7] and Indonesia earthquake in 2018 [8] led to liquefaction related failures and damages to urban areas. Lastly, the twin Maras earthquake events on the 6th of March 2023 caused liquefaction related building failures in many affected areas, especially in Gölbaşı (Adıyaman) and Iskenderun (Hatay) districts [9, 10].

Occurrences of earthquake events featured by aleatory uncertainty are sudden and unforeseen, therefore the liquefaction triggering at any site [11]. However, this random uncertain natural event and, specifically, its cause of liquefaction, at a specific site should have to be determined in order to; (1) mitigate such effect on mainly buildings, bridges, roads and buried pipelines, (2) realise seismic hazard risks and (3) planning of the urban areas [12]. Hence, characterisations of sites regarding the liquefaction potential under possible earthquake events gained great interest of geotechnical and geological engineering communities.

Liquefaction potential of a given site can often be determined based on laboratory and field tests. Laboratory test results are always regarded as sceptical since taking samples from the soil ground, transporting to the laboratories and placing the samples to the test machines may disturb the original soil structures [13, 14]. In contrast, field tests produce relatively more sustainable soil data free from the issues confronted in laboratory tests [2]. Hence, field tests have seen as better choice over the laboratory tests. Common field tests practised with the aim of delineating liquefaction potential of soil layers are Cone Penetration Test (CPT), Standard Penetration Test (SPT) and Becker Penetration Test along with the shear wave velocity (V_s) measurement techniques. When CPT test and V_s measurement can still convey the liquefaction potential of the soils [15-16], SPT based liquefaction assessments are overwhelmingly applied in geotechnical and geological engineering studies [18-20]. In this regard, the study conducted by [2] presented the liquefaction potential in the Kahramanmaraş city situated on the East Anatolian and Dead Sea Faults. They used 238 geotechnical boreholes to analyze and map the liquefaction risk over the city. In addition, the city of Erzincan was also studied for the liquefaction potential under different seismic intensities [21]. Since the city is positioned close to the both main fault lines (North Anatolian and East Anatolian fault lines), the study clearly indicated the liquefaction potential by utilizing the SPT data. Moreover, the liquefaction potential of Battalgazi region (in the Malatya city sitting nearby the East Anatolian Fault) was evaluated, along with the site amplification, based on the measured SPT values [22]. The V_s and SPT based liquefaction assessments were also made for Erzurum (Van) as the liquefaction cases were observed during the October 23, 2011, Van earthquake [23]. The predictions of the study were shown to represent the actual scenarios.

Specific focus of this study is an urban area of Igdir province in the eastern Anatolian region of Türkiye. It aims to map the liquefaction potential of the location based on in-situ test results. The area falls within the Ararat Basin, which was created by the geological shifts of the Eurasian and Arabian plate boundaries, along with other nearby basins such as Rioni, Kura, Mid-Araks, and Nakhichevan [24]. The Ararat Basin is bordered to the northwest by the Aragats and Gegham volcanic formations and to the south by the volcanic Mount Ararat. The area is located on quaternary alluvium and surrounded by sedimentary rocks (i.e., slope debris, alluvial fan deposits, and moraines) as well as clastic rocks. Moreover, volcanic rocks such as basalt and andesite are present towards Mount Ararat. Since the province neighbors with Armenia in the north-east, Nakhichevan in the south-east and Iran in the south, its location is one of the unique geographical locations in the world. The province is also growing in terms of population, as at the beginning of the century, it has 174 285 population and in 2022 the population reaches to 203 594 by almost %17 of increase [25]. Due to its distinctive position suitable for trade and therefore for industrial developments, the growing population is likely to rise even more rapidly. Thus, mapping the liquefaction of the three different parts of the city, which has not been conducted before, can be beneficial in mitigating seismic effect of possible future earthquake events, depicting seismic hazard risks and for future planning. The geological maps presented throughout the paper are produced by means of geographic information systems (GIS) software. The paper carries on with describing the location and its seismicity in details. In addition, the locations of SPT boreholes are illustrated. Subsequently, the methods used to delineate the liquefaction potential of the site are presented. Lastly, the liquefaction maps of the studied area are interpreted with some comparisons.

2. Location of Iğdır province

The Iğdır province is positioned in between approximately 39°- 41° latitude northerly and 43°-45° longitude easterly [26]. The considered study site is the urban area of the Iğdır province covering the city centre as shown in Figure 1. The province consist of mostly mountainous fields, but almost %30 of the area formed by plain land, so called Iğdır plain. The population, including the main city, has largely been settling in the plain area. The plain remains between Mount Ararat and the Caucasus Mountains causing the plain to be featured with the bowl-shape structure [27].

The soil of the plain region is characterised substantially by quaternary alluvial soils covering a land of around 922 km². The alluvial soil is formed over time by the depressions of Aras river connected with various straits. In fact, Aras River is accepted as border between Türkiye and Armenia and is the main cause of recent soil formations in Iğdır plain at the Türkiye side, and Revan plain at the Armenian side, with almost equal sizes. These two plain areas are sit on top of Surmeli and Sahat concavities at the Türkiye and Armenian sides, respectively [28].

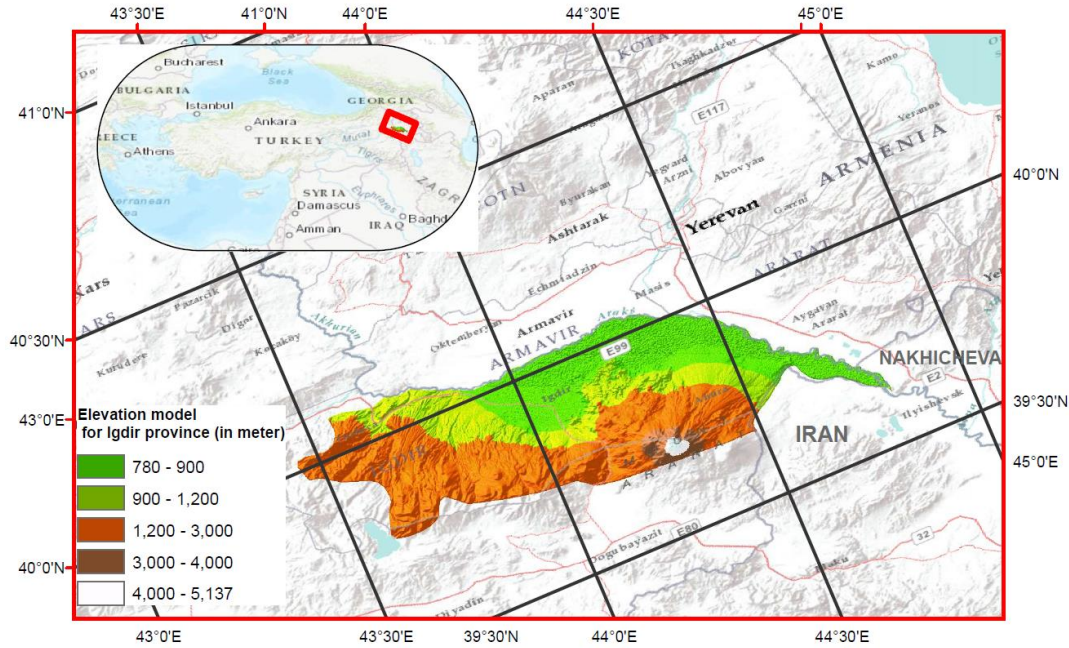


Figure 1. Elevation model for the Iğdır province demonstrating the mountainous and plain areas

3. Seismicity of the Site

Türkiye is known as one of the seismically active countries in the world, as it sits on top of mostly Anatolian and partially Arabian and Eurasian plates. As a result of relative movement of Arabian plate toward northwards with a rate of 6-10 mm per year, Anatolian plate is pushed to the westwards with a rate of 18.7- 21.5 mm per year [29, 30]. The contrast between these three plates create two main fault lines, recognised as North Anatolian Fault Zone (NAFZ) and East Anatolian Fault Zone (EAFZ). Moreover, these tectonic plates are the causes of many fault lines formed over the countries of Türkiye, Greece, Armenia and Iran.

Within 100 km distance in radius from the Iğdır city center, there has been, in total, 89 earthquake events recorded with magnitudes greater than or equal to 4.00 [31]. The epicenter of the events are illustrated in Figure 2. The number of earthquake events taken place within the scale at different magnitude ranges is presented in Table 1. It is clear that, as the magnitude range increases, the occurrence of such event reduces. For instance, at 4-4.50 and 4.50-5.00 magnitude ranges, 45 and 20 earthquake events have been recorded when only 9 and 5 records are available at 5.00-5.50 and higher than 5.50, accordingly. In other words, the small magnitude earthquake events are frequent and but less destructive, while the big earthquake events are relatively rare but more destructive and pertinent.

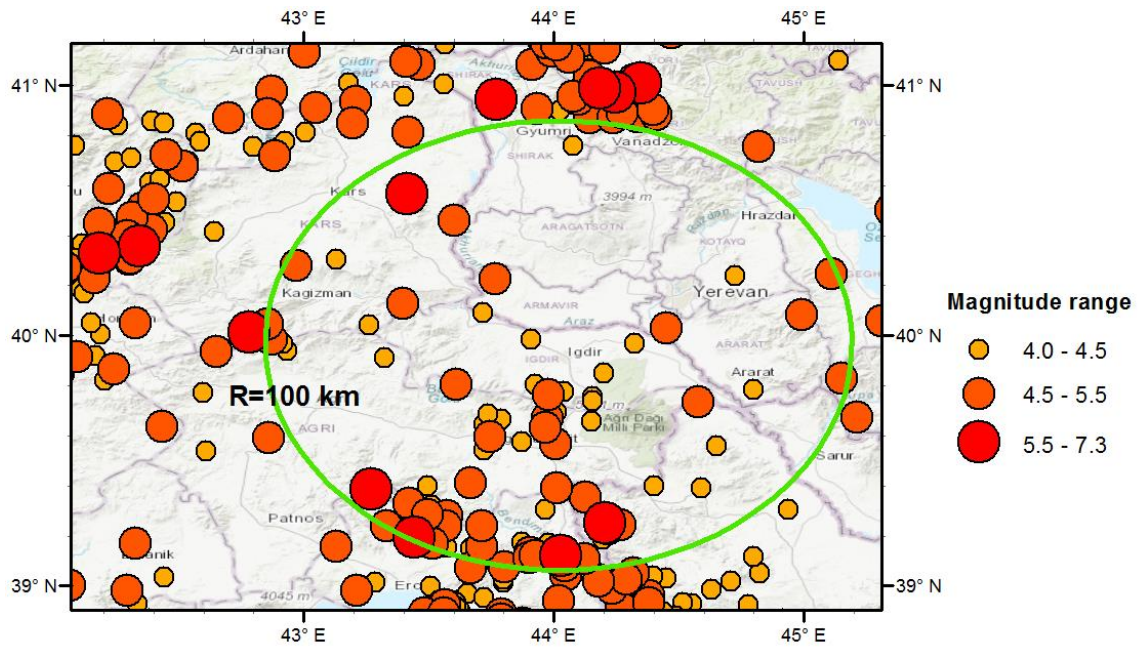


Figure 2. Location of past earthquake events taken place around the area of interest including the circle centered by 100 km in radius from the Iğdır city center

Table 1. Number of past earthquake events at various magnitude ranges occurred within the 100 km radius around the Iğdır city center

Magnitude range	4.00-4.50	4.50-5.00	5.00-5.50	>5.50
Number of event	45	20	9	5

Several active earthquake fault lines surrounding Iğdır city are demonstrated in Figure 3. It is important to stress here that only active fault lines in the Türkiye side, which have relatively recently been updated by Emre et al. [32], is considered as can be depicted from the figure. Active fault lines in the Armenia, Nakhcivan and Iran sides neighboring the Iğdır province are not presented since up-to-date active fault lines are not available. In fact, an extensive study carried out in 2004 by Karakhanian et al. [33] focused on fault lines and past earthquake events occurred over those lines in Armenia, eastern Türkiye and northwestern Iran. However, the presented fault lines in the aforementioned study, in the eastern Türkiye covering the study area, were significantly changed when compared with the active fault lines presented in Figure 3. Such changes may also be conceivable for the active faults in the neighboring countries. Therefore, the fault lines at the neighboring countries and hence any likely possible earthquake events are not taken into consideration in this study.

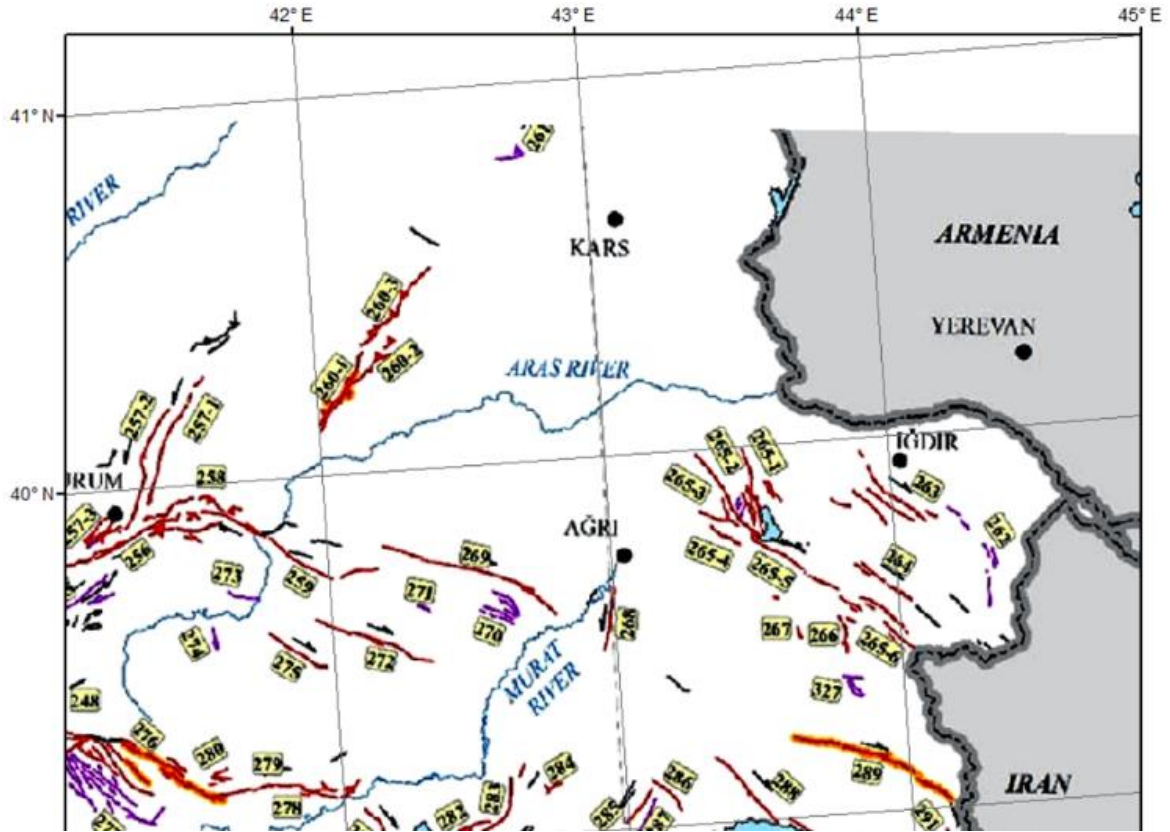


Figure 3. Active fault lines around the studied area of Iğdır [25]

The nearest fault line called Iğdır Fault Zone with ID of 263, is just about 7.40 km distance to the area of interest. In addition, there are other active fault lines whose locations are shown in Figure 3 which may trigger earthquake events that may cause some level of hazards in the study area. General properties of the fault lines are given in Table 2. In order to determine largest earthquake event likely to occur at the active fault lines, the equation proposed by Wells and Coppersmith [34] is applied. The equation depicts the moment magnitude (M_w) by relying on the surface rupture length (SRL).

$$M_w = 5.08 + 1.16 \log (SRL) \quad (1)$$

Based on this equation, it is clear that magnitude of an earthquake event to be happened over the fault line depends on its length. Therefore, the highest magnitude earthquake event is likely to occur in the Perilidag Section with M_w of 6.83, followed by Tirso Gölü Section with M_w of 6.80 and Iğdır Fault Zone with M_w of 6.78 for the fault line lengths of 32 km, 30 km and 29 km, respectively. Magnitudes of potential earthquake events at the other fault lines are included in Table 2.

Table 2. Active fault lines around the studied area and the largest possible earthquake events possible to take place along these faults

Fault Name	ID	Type	Length	M_w	Distance to the study area (km)	PGA (g)	
	Iğdır FZ	263	RL	29	6.78	7.40	0.393
Dogubeyazit F	264	RL	20	6.60	28.85	0.126	
Ağrı EF	262-3	NN	11	6.30	17.00	0.225	
	262-1	NN	8	6.13	32.74	0.140	
	262-2	NN	9	6.19	41.40	0.122	
Bahıngölü FZ	Candeviş S	265-1	RL	25	6.70	35.80	0.200
	Perilidag S	265-2	RL	32	6.83	41.40	0.194
	Kovancık S	265-3	RL	10	6.24	43.73	0.120
	Tirso Gölü S	265-4	RL	30	6.80	49.90	0.160
	Yeni Cadır S	265-5	RL	17	6.50	38.50	0.163
	Cetenli S	265-6	RL	18	6.54	38.83	0.166

FZ; Fault Zone, F; Fault, EF; Extensional fissure, S; Segment, RL; Right Lateral, NN; Normal

The peak ground accelerations (PGA or a_{max}) likely to be experienced at the studied area due to the predicted earthquake events should be determined. This is because of the fact that the magnitude of an earthquake event can demonstrate its energy level, but cannot give any indication of its hazards to the considered area. In contrast, PGA can better illustrate the impact level of such event. In particular, the prediction of PGA is necessary to represent the liquefaction potential of the area. While there are several ground motion attenuation equations proposed to predict PGA, this study utilised the one developed by Ulusay, Tuncay [35] based on the local-based (Türkiye) earthquake data. The associated ground motion prediction equation is given below.

$$PGA = 2.18e^{0.0218(33.3M_w - R_e + 7.8427S_A + 18.9282S_B)} \quad (2)$$

in which, $S_A=0$, $S_B=0$ for rock, $S_A=1$, $S_B=0$ for stiff soil and $S_A=0$, $S_B=1$ for loose soil. R_e is a distance measured from the closest point of the fault line to the area of interest. In this sense, considering the magnitude level of a potential earthquake event at the Igdir Fault Zone and its closeness to the study area with just about 7.5 km, it may cause the largest PGA, that is equal to 0.393g, at the site. Second largest PGA of 0.225g may be recorded, when an earthquake event is triggered at the Agri Extension Fissure (fault ID of 262-3), as tabulated in Table 2. This is followed by the any likely earthquake event at the two sections of the Balıkgölü Fault Zone (i.e. Candervis Section with fault ID of 265-1 and Perilidag Section with fault ID of 265-2) resulting in PGA of 0.20g and 0.194g at the site, respectively. Other potential PGA at the study area under foreseeable earthquake events at the regarded fault lines are given in Table 2. Important to note here that the maximum probable PGA in 475 years of return period (%10 probability of exceedance in 50 years) is given as, on average, around 0.25g for the studied area (Ministry of Disaster and Emergency Management Presidency (AFAD) [31]), which is distinctively lower than the maximum PGA predicted from the deterministic approach. Therefore, this study considers only first two highest possible PGA values that are 0.393g and 0.225g calculated based on the above deterministic approach. Considering the fault lines around the study area from Türkiye side as well as from Armenian side, adapting deterministic approach may be more reliable in assessing the liquefaction potential.

4. Study Areas and Geotechnical Features

In this study, three separate regions called as Area_1, Area_2 and Area_3 at Igdir city are taken into consideration, as highlighted in Figure 4. While the Area_1 involves only Yeni Mahalle district, the Area_2 and the Area_3 consist of Konakli, 7 Kasim, Ozgur, Konakli and Karaagac districts and Emekli, Alikemerli and Hakveyis districts, respectively. The studied Area_1 covers approximately 1.00 km², the Area_2 and the Area_3 occupy lands of 4.50 km² and 3.40 km², accordingly. As the geotechnical data is attained from the local municipality (Igdir), the data is esteemed to be reliable to conduct this study.

In total, 85 boreholes were opened to investigate the geotechnical characteristics of the areas. 68 boreholes were explored until the depth of 15 m, when only 17 boreholes extend to the depth of 20 m. Mainly, grain-size distribution, Atterberg limits, unit weight, ground water levels and Standard Penetration Test values (SPT-N) were determined. The soils were classified in compliance with the Unified Soil Classification System (USCS). From the sieve analysis, the soil layers are characterised by mostly fine grained soils comprising %75 of the total soil bodies and partially by coarse grained soils encompassing %25 of the total soil bodies. Fine grained soil layers are made of low or high plastic clay and silt with the inclusions of gravel and sand soils. Similarly, coarse grained soil layers include mainly sand and occasionally gravel involving silt and clay materials. The maximum-minimum plastic limit (PL) and liquid limit (LL) values available for the characterised soils equal to 77.9-26.2 (%) and 42.1-12.4 (%), respectively. The water content of the soils at the site ranges from 1.7 (%), realised above the water table to 57 (%) as maximum available below the water table. The soil densities measured were varied between 17.7 kN/m³ and 19.2 kN/m³.

The water levels at the boreholes get mostly as low as to 1.5 m from the ground surface, and reaches to 5 m at several locations. Water table distributions within the studied areas are illustrated in Figure 5. It is clear that the water table measured at all boreholes within the Area_1 varies only between 1.5 m and 2.00 m (Figure 5a), while, within the Area_2, it ranges from 1.50 m to 2.00 m (Figure 5b). The water levels at the Area_3 are mostly varies between 4.00 m to 5.00 m, as seen in Figure 5c, when only 3, 1 and 2 boreholes kept water tables at 1.50-2.00 m, 2.00-3.00 m and 3.00-4.00 m depth ranges. The measured SPT-N values at the boreholes extended from 3 to 51. In general, the SPT-N values increased with depth, but fluctuate at some boreholes as encountered with relatively softer soil layers. Three SPT-N profiles (one borehole in each area) and their changes through the borehole depths are demonstrated as an example along with the correlated shear wave velocity (V_s) values in Figure 6. The recent

study conducted by Guzel [36] provides correlation between SPT-N and shear wave velocity (V_s) values for the area, as such:

$$V_s = 199N^{0.0626} \quad (3)$$

The average V_s values at the associated boreholes are 243.35 m/s, 244 m/s and 230 m/s, respectively.

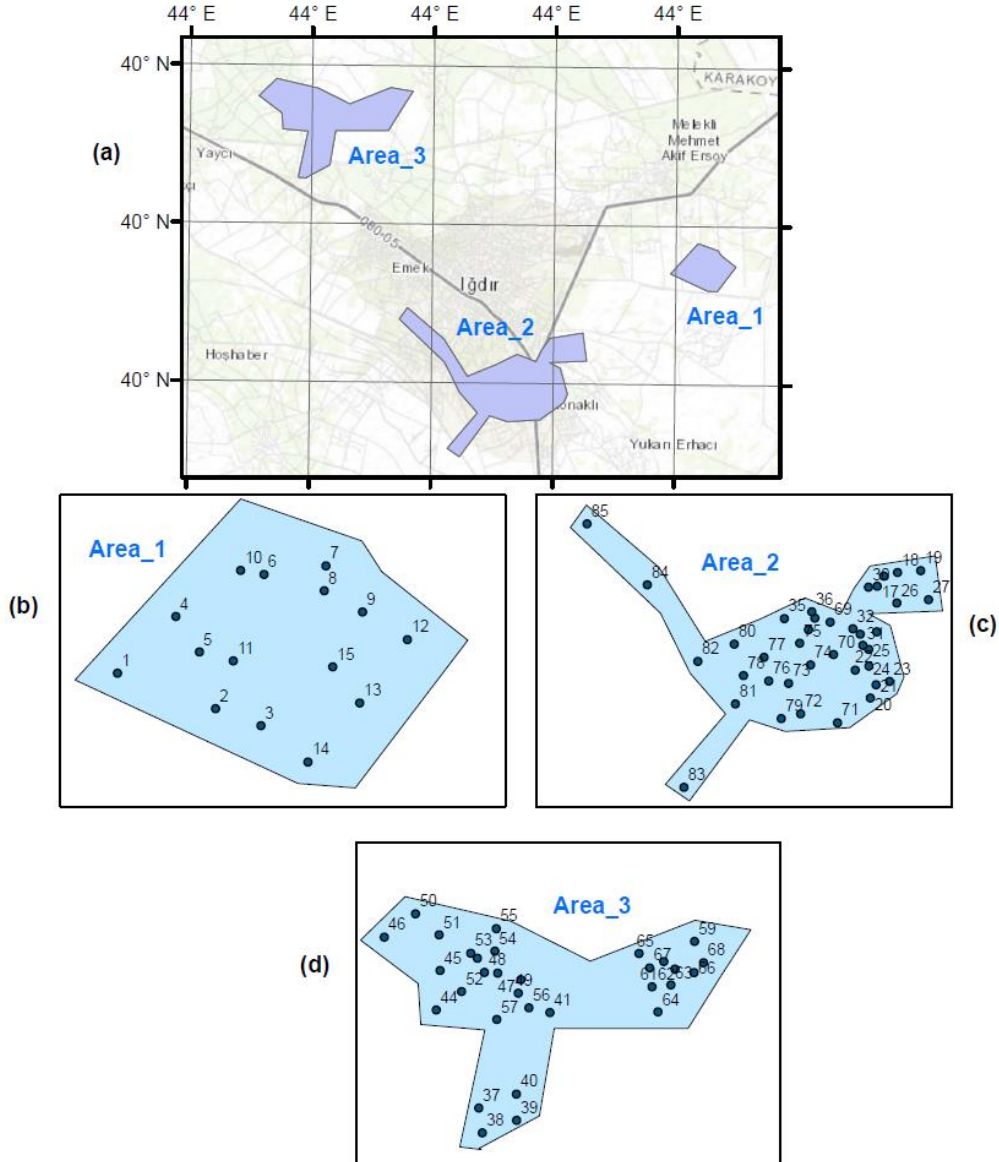


Figure 4. (a) Borders and Locations of the studied areas within the Igdir city, (b) positions of the boreholes within the Area_1, (c) positions of the boreholes within the Area_2 and (d) positions of the boreholes within the Area_3

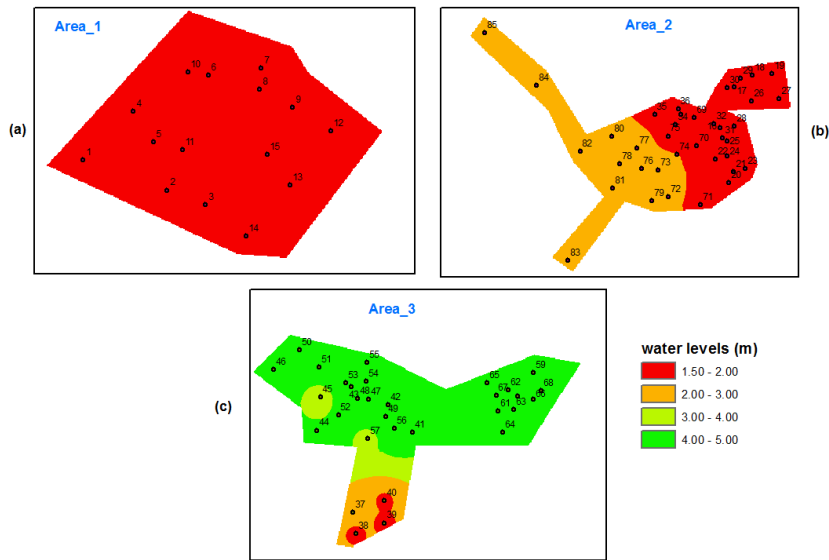


Figure 5. Water level distributions over the studied Area_1 (a), Area_2 (b) and Area_3 (c) based on the measured water levels at the associated boreholes

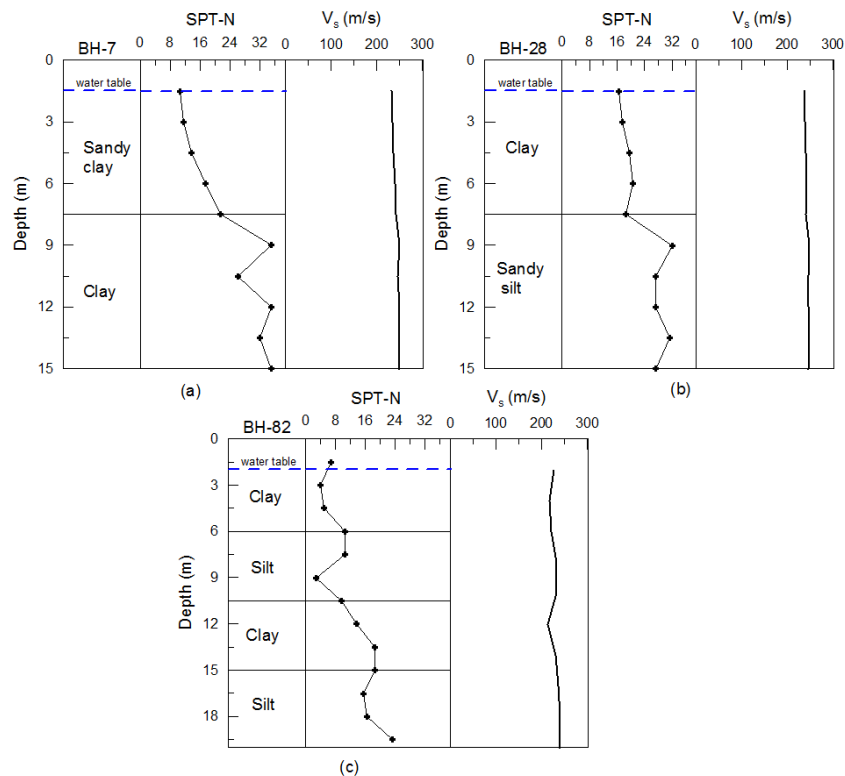


Figure 6. Three exemplary SPT-N profiles and correlated V_s values located in; (a) Area_1 (BH-7), (b) Area_2 (BH-28) and (c) Area_3 (BH_82)

5. SPT Based Liquefaction Assessment Methods

The liquefaction potential of a soil layer can be assessed through laboratory testing or on-site test methods, as well as through empirical techniques. Empirical methods, which rely on on-site penetration testing, are commonly utilized because of the challenges of obtaining appropriate soil samples testing on laboratory environments. The Standard Penetration Test (SPT) is a popular in situ test choice for evaluating the risk of liquefaction, and is widely used in many countries, including Türkiye. In this study, the potential for liquefaction was analyzed using the simplified SPT-based method introduced by Seed and Idriss [37] and Seed et al. [38]. The modifications suggested by Youd et al. [19] were also considered. The corrected SPT-N values were calculated using the equation provided by Liao and Whitman [39]. The cyclic stress ratio (CSR), defined as the amount of cyclic shear stress needed to cause liquefaction, was first proposed by Seed and Idriss [18]. Youd et al. [19] made a slight modification to the calculation of CSR. Seed et al. in 1985 presented an empirical correlation between corrected $SPT(N_1)_{60}$ and CSR. The empirical correlation curves, which are the same as the liquefaction triggering curves, depict the capacity of

soil to resist liquefaction, referred to as the cyclic resistance ratio (CRR). Youd et al. [19] modified the CRR curves from Seed et al. [38], including those for clean sands and magnitude 7.5 earthquakes. The CRR curves provide the limiting conditions for determining if liquefaction will occur for a magnitude 7.5 earthquake. Moreover, CRR curves were developed for granular soils with fine contents of %5 or less, %15, and %35 [19].

In this study, the Cyclic Resistance Ratio (CRR) equation proposed by Youd et al. [19] was used. To evaluate the risk of liquefaction, a factor of safety (F_s) equation was developed, which considers $CRR_{7.5}$, Cyclic Stress Ratio (CSR), and Maximum Scaling Factor (MSF) as represented by the following formula:

$$F_s = (CRR_{7.5}/CSR)MSF \quad (3)$$

The Magnitude Scaling Factor (MSF) was utilized as described in Eq. 4 [19].

$$MSF = \frac{10^{2.24}}{M_w^{2.56}} \quad (4)$$

CRR and CSR were calculated based on the equations originally given by Seed et al. [38]:

$$CRR_{7.5} = \frac{1}{34 - (N_1)_{60}} + \frac{(N_1)_{60}}{135} + \frac{50}{[10(N_1)_{60} + 45]^2} - \frac{1}{200} \quad (5)$$

$$CSR = 0.65(\alpha_{max}/g)(\sigma_{vo}/\sigma'_{vo})r_d \quad (6)$$

In which, α_{max} is the maximum ground acceleration, g is the acceleration of gravity, σ_{vo} and σ'_{vo} are total and effective overburden stresses and r_d is the stress reduction coefficient. The value of r_d is computed from the following depth- dependent equations:

$$\begin{aligned} r_d &= 1 - 0.00765z \text{ for } z \leq 9.15 \text{ m} \\ r_d &= 1.174 - 0.0267z \text{ for } 9.15 \text{ m} < z \leq 23 \text{ m} \end{aligned} \quad (6)$$

$(N_1)_{60}$ in the Equation 5 is the corrected SPT-N (N_{30}) and obtained by using;

$$(N_1)_{60} = N_m C_N C_E C_B C_R C_S \quad (7)$$

In which, N_m : the measured standard penetration counts, C_N : normalization of N_m with respect to the reference overburden pressure, C_E : hammer energy efficiency level, C_R : rod length dependent correction factor, C_S : borehole sampler correction. The overburden pressure correction factor, C_N , is calculated regarding the equation proposed by Liao and Whitman [39]:

$$C_N = \left(\frac{P_a}{\sigma'_{vo}}\right)^{0.5} \quad (8)$$

Where, P_a is an atmospheric pressure of 100 kPa (1 atm) and σ'_{vo} is the effective overburden pressure. This value cannot exceed 1.70. Besides, since the amount of fine content involved in clean sand is shown to alter the liquefaction resistance of the soil, following fine content (FC) corrections are recommended.

$$(N_1)_{60cs} = \alpha + \beta(N_1)_{60} \quad (9)$$

In which, α and β coefficients are determined regarding the extent of fine content inclusions, as:

$$\begin{aligned} FC \leq \%5, & \quad \alpha = 0 \text{ and } \beta = 1 \\ \%5 < FC \leq \%35, & \quad \alpha = \exp\left[1.76 - \left(\frac{190}{FC^2}\right)\right] \text{ and } \beta = [0.99 + (FC^{1.5}/1000)] \\ FC \geq \%35, & \quad \alpha = 5 \text{ and } \beta = 1.2 \end{aligned} \quad (10)$$

In the literature, the susceptibility of loose sand layers to liquefaction has been investigated up to a depth of 20 meters from the surface [37-42]. According to various studies, liquefaction occurs when the factor of safety is less than 1.0. Additionally, it is stated that the factor of safety ranging from 1.0 to 1.2 defines the liquefaction as marginally liquefiable, but no liquefaction will occur when the factor of safety is above 1.2 [42-44]. However, Seed and Idriss [46] noted that the acceptable factor of safety value for the liquefaction phenomenon is between 1.25 and 1.5.

Iwasaki et al. [47] introduced a liquefaction potential index (LPI) to overcome the limitations of the factor of safety (F_s). The LPI is divided into four categories of liquefaction potential, including very low, low, high, and very high, and is calculated using the following equations (Eqs. 11a, b, c, d and e).

$$LPI = \int_0^{20} F(z)W(z)dz, \quad (11a)$$

$$F(z) = 1 - F_L \text{ for } F_L < 1.0, \quad (11b)$$

$$F(z) = 0 \text{ for } F_L \geq 1.0, \quad (11c)$$

$$W(z) = 10 - 0.5z \text{ for } z < 20m, \quad (11d)$$

$$W(z) = 0 \text{ for } z \geq 20m \quad (11e)$$

The depth of the soil layer is represented by z , measured in meters, and F_L represents the factor of safety against liquefaction and equals to F_s . The classification of liquefaction potential is defined by the boundary values of the liquefaction potential index (LPI) which are presented in Table 3 along with the liquefaction susceptibility descriptions.

Table 3. Liquefaction potential classification suggested by Iwasaki et al. [47]

Liquefaction index (LPI)	Description
0	Very Low
$0 < LPI \leq 5$	Low
$5 < LPI \leq 15$	High
$15 > LPI$	Very high

$$F(z) = 0 \text{ for } F_L \geq 1.2, \quad (12a)$$

$$F(z) = 2 \times 10^6 e^{-18.427F_L} \text{ for } 1.2 > F_L > 0.95, \quad (12b)$$

$$F(z) = 1 - F_L \text{ for } F_L < 0.95 \quad (12c)$$

The probability of soil liquefaction (P_L) depends on the value of F . Sonmez and Gokceoglu [48] proposed the liquefaction severity index (L_s), and they preferred to use the P_L value in this index equation. According to Sonmez and Gokceoglu [48], it is believed that the use of a liquefaction probability equation in the calculation of a liquefaction index will provide more consistency. The liquefaction severity index (L_s) is calculated using the following equations (Eqs. 13a, b, c, d and e).

$$L_s = \int_0^{20} P_L(z)W(z)dz, \quad (13a)$$

$$P_L = \frac{1}{1+(F_L/0.96)^{4.5}} \text{ for } F_L \leq 1.411, \quad (13b)$$

$$P_L(z) = 0 \text{ for } F_L > 1.411, \quad (13c)$$

$$W(z) = 10 - 0.5z \text{ for } z < 20m, \quad (13d)$$

$$W(z) = 0 \text{ for } z \geq 20m \quad (13e)$$

The depth of the midpoint of the soil layer is represented by z and the factor of safety against liquefaction is represented by F_L in Eq. (13) for the calculation of the liquefaction severity index (L_s). The boundary values for L_s , along with descriptions of liquefaction susceptibility, are presented in Table 4.

Table 4. Liquefaction severity index value ranges

Liquefaction severity (L_s)	Description
$85 \leq L_s < 100$	Very High
$65 \leq L_s < 85$	High
$35 \leq L_s < 65$	Moderate
$15 \leq L_s < 35$	Low
$0 \leq L_s < 15$	Very Low
$L_s = 0$	Non-Liquefiable

6. Results and Discussions

6.1. SPT versus Cyclic Stress Ratio

The corrected $SPT(N_1)_{60}$ values and corresponding CSR values at 0.393g and 0.225g seismic intensity levels are plotted in Figure 7 along with the modified CRR curves given by Youd et al. [19]. The boundary CRR curves in Figure 7 are determined by the fine content of the granular soil (i.e. being higher than 35%, between 35% and 5%

and less than 5%) and, therefore, separates the graph into three regions. The curves are developed based on historical cases. For the PGA level of 0.393g, out of the 46 data, 17 of them fall into the liquefaction region, over the %35 fine content CRR curve. Only 3 of the soil data are between %35 and %15 fine content CRR curves and 12 of them are represented between %15 and %5 fine content CRR curves. For the lower PGA level (i.e., 0.225g), the number of soil data likely to experience liquefaction is reduced. For instance, only the 5 soil data are over the %35 fine content CRR curve and only the 10 soil data are fitted between the CRR curves. This is obviously due to the fact that the stress on soil induced by the 0.393g seismic intensity is greater than the stress caused by the 0.225g seismic intensity.

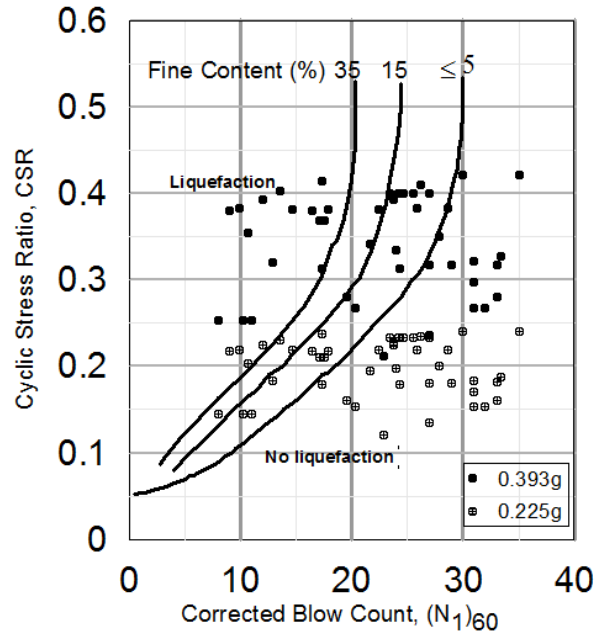


Figure 7. Computed cyclic stress ratio (CSR) with the measured SPT $(N_1)_{60}$ values at the 0.393g and 0.225g seismic intensity levels and cyclic resistance ratio (CRR) based on Youd et al. [19]

6.2. Liquefaction potential in regard to fine content

Additionally, hydrometer and Atterberg limits experiments were conducted on 288 soil samples obtained from various depths of 85 boreholes in alluvial deposit areas. The liquefaction potential of these soils (specifically in fine-grained soil layers) was also assessed using the method proposed by Seed et al. [41] (as shown in Figure 8). It is clear from the figure that the low-plastic silt soils (and also low-plastic silt soils with clay) are regarded to be susceptible to liquefaction. On the contrary, low- and high-plastic clay soils and high-plastic silt layers are unlikely to liquefy. Based on this method, 24 samples were classified into region A and 87 samples were classified into region B (as seen in Figure 8). Therefore, the fine-grained soil layers exist in the area also hold liquefaction potential.

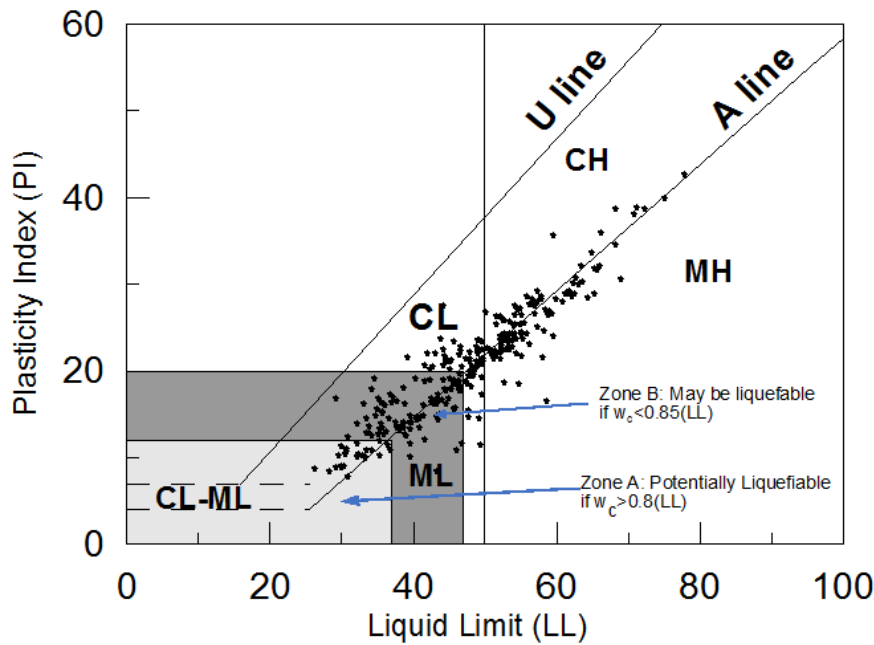


Figure 8. Liquefaction potential silty soil layers at the studied boreholes as described by Seed et al. [41]

6.3. Mapping of liquefaction potential

Liquefaction potential of the studied areas are assessed with respect to the two methods described in the previous section (LPI and L_s), mentioned in the previous section, suggested by Iwasaki et. al. [47] and Sonmez and Gokceoglu [48]. The two highest PGA values of 0.393g and 0.225g that can be recorded at the site in future are regarded when the liquefaction potentials are mapped. The maps presented in this section are produced by means of geographic information systems (GIS) software. The computed LPI and L_s at SPT locations are interpolated with inverse distance weight (IDW) method. The interpolation method estimates the desired values at a location from the measured values at known certain locations by allocating weight values based on their distances to the location of estimate.

Based on the LPI values, likelihood of liquefaction occurrence within the Area_1 can be categorized as high, as demonstrated in Figure 9a. Only at three boreholes (BH-1, BH-5 and BH-9) the liquefaction potential is low as exact LPI values are 4.67, 4.54 and 4.19, respectively (as presented in Table 5). It is very high at only BH-7 with exact LPI value of 16.50. Besides, most part of the Area_2 is likely to experience liquefaction at very high or high levels, when the area is shaken by an earthquake event with PGA level of 0.393g (Figure 9b). The liquefaction potential is seen as low at 5 boreholes (BH-21, BH-23, BH-34, BH-35 and BH-36) in the same area since the computed LPI values are lower than 5, as seen in Figure 9b and Table 5. In contrast, in the north-west side of the city (Area_3), the liquefaction potential is very low, as LPI values obtained at all of the boreholes are equal to 0 or less than 5.00 (shown in Figure 9c and Table 5).

The liquefaction assessments of the areas with respect to the L_s values express less degree of liquefaction occurrence when compared with the LPI based assessment method under the same seismic intensity level. More specifically, the Area_1, in contrast to the liquefaction potential being high with respect to the LPI values, is characterized by low liquefaction severity (Figure 10a). The Area_3 is symbolized by non-liquefiable or very low liquefaction potential (Figure 10c), as in the case of LPI based method. The Area_2, though, is very likely to encounter liquefaction effect extending from mostly high level to moderate level, as can be depicted from Figure 10b. The liquefaction potential at the remaining area is dominantly low and only very low at 5 boreholes (BH-21, BH-23, BH-34, BH-35 and BH-36). However, most of the Area_2 is at very high level of liquefaction potential risk when the LPI values are regarded.

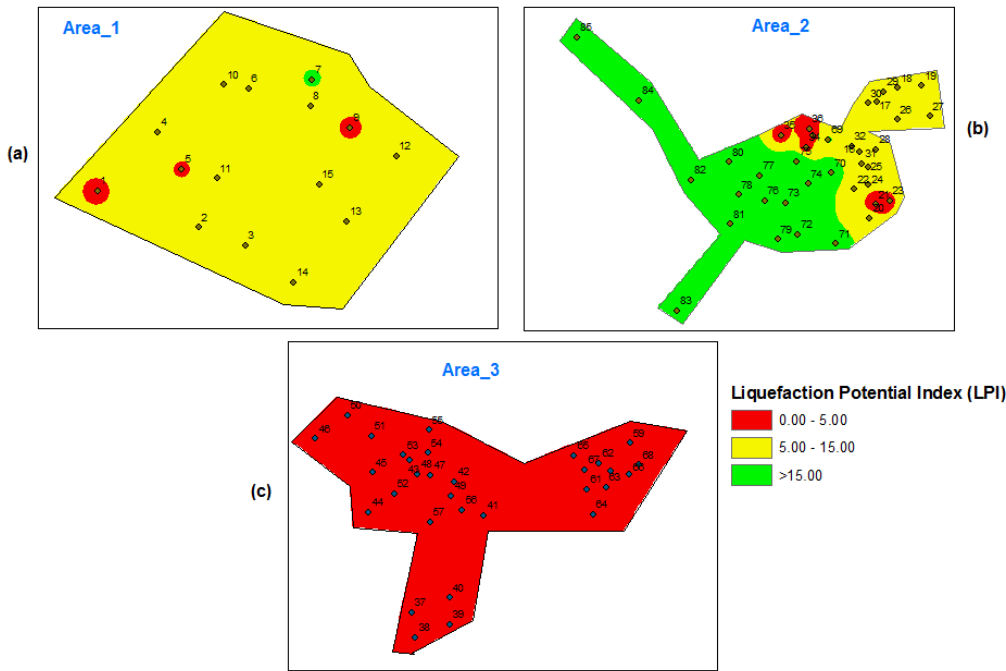


Figure 9. Liquefaction Potential Index (LPI) of the studied areas when 0.393g peak ground acceleration is considered

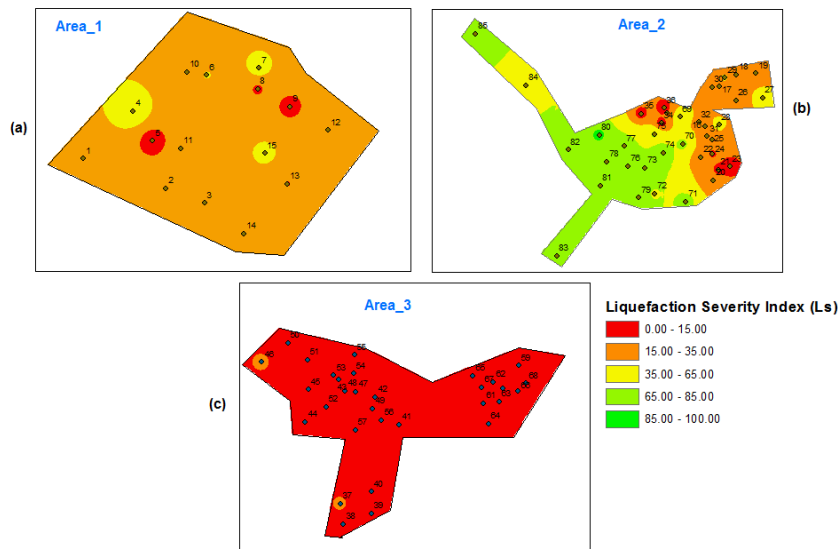


Figure 10. Liquefaction Severity Index (L_s) of the studied areas when 0.393g peak ground acceleration is considered

In the case of implementing the second largest possible peak ground acceleration, the investigated areas are less likely to experience liquefaction at the greater extent as the examined PGA reduces from 0.393g to 0.225g. Specifically, the Area_1, Area_3 and most part of the Area_2 own very low level of LPI values being 0 or less than 5 (can be seen in Figures 11a-c and Table 5). In the area_2, only at 7 boreholes (BH-72, BH-75, BH-77, BH-80, BH-84 and BH-85) possess high level of liquefaction which can be observed from Figure 11b and Table 5. The LPI values at these boreholes are 6.03, 8.31, 5.65, 11.98, 5.21 and 7.05, respectively. In the same way, the L_s values for the Area_1 and Area_3 suggest very low liquefaction severity (Figures 12a, c). However, at the large parts of the Area_2, there is still moderate and low levels of liquefaction severity since the L_s values extend from 15 to 65 while the remaining part of the area is very low level of liquefaction potential (Figure 12b). It is clear from Figure 11b and Figure 12b that the same part of the Area_2 expresses greater level of liquefaction potential in terms of than the remaining part. This implies that although the LPI and L_s based liquefaction evaluation methods are different, they can still leads to similar liquefaction potential indication, hence, in a way validate each other.

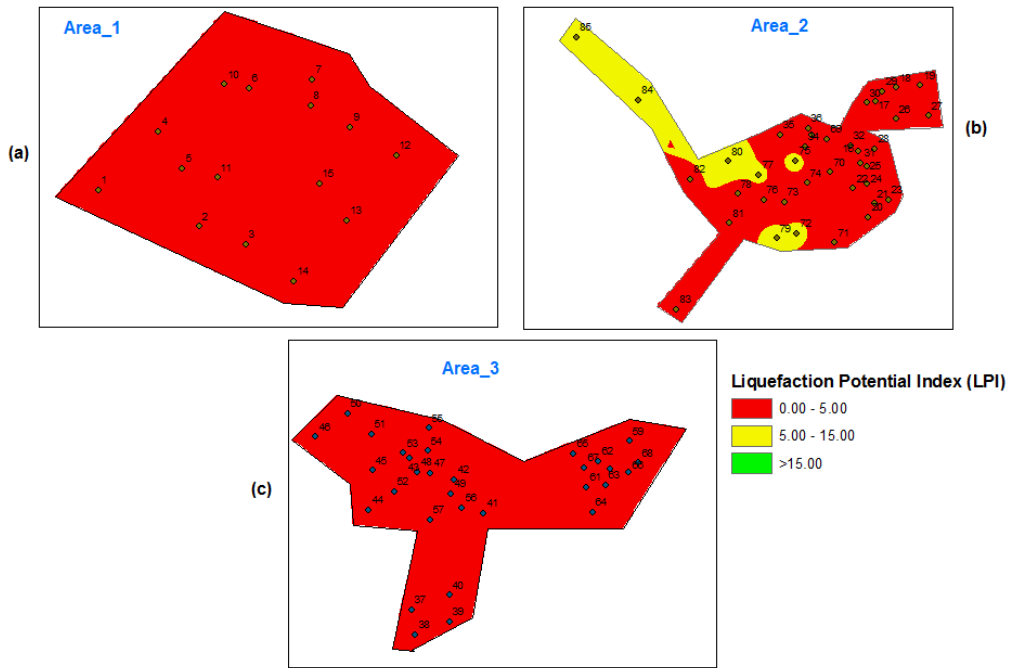


Figure 11. Liquefaction Potential Index (LPI) of the studied areas when 0.225g peak ground acceleration is considered

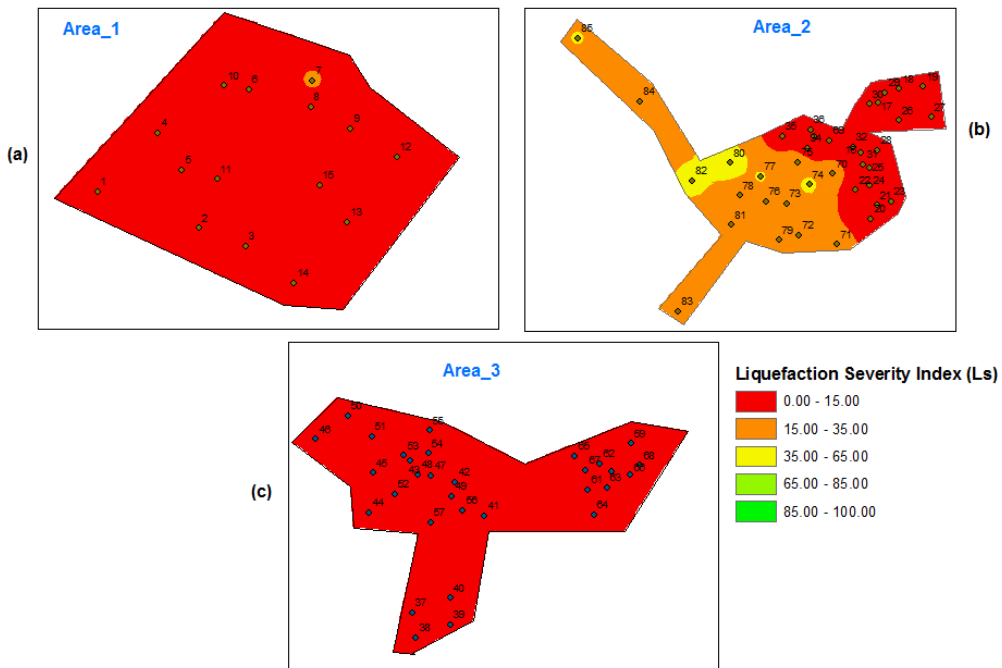


Figure 12. Liquefaction Severity Index (Ls) of the studied areas when 0.225g peak ground acceleration is considered

Table 5. Locations and liquefaction potentials at the boreholes in terms of LPI and LS values

Borehole_no	coordinates		LPI	Describ.	L _s	Describ.	LPI	Describ.	L _s	Describ.
	easting	northing								
BH-1	423135.1	4419672	4.67	Low	17.47	Low	0.00	Low	3.45	Very low
BH -2	423514.3	4419534	7.71	High	25.06	Low	0.36	Low	6.97	Very low
BH -3	423689.4	4419468	6.73	High	17.75	Low	0.64	Low	7.30	Very low
BH -4	423361.2	4419891	12.69	High	53.38	Moderate	1.65	Low	9.72	Very low
BH -5	423452.3	4419754	4.54	Low	7.16	Low	0.00	Low	3.90	Very low
BH -6	423701.5	4420054	8.40	High	35.72	Moderate	2.01	Low	8.96	Very low
BH -7	423941.5	4420087	16.50	Very high	43.01	Moderate	2.30	Low	16.49	Low
BH -8	423934.5	4419991	6.38	High	13.28	Very low	0.36	Low	6.97	Very low

Liquefaction Hazard Assessments in Igdir City (Türkiye)

BH -9	424082.5	4419909	4.19	Low	11.49	Very low	0.00	Low	3.47	Very low
BH -10	423611.3	4420069	5.22	High	16.99	Low	0.00	Low	4.88	Very low
BH -11	423583.3	4419719	6.30	High	19.62	Low	0.00	Low	5.43	Very low
BH -12	424256.6	4419802	7.04	High	28.69	Low	0.64	Low	7.30	Very low
BH -13	424071.5	4419556	6.79	High	14.82	Very low	0.08	Low	6.64	Very low
BH -14	423871.4	4419328	6.49	High	21.34	Low	0.36	Low	6.97	Very low
BH -15	423967.5	4419697	11.28	High	39.85	Moderate	1.48	Low	8.30	Very low
BH -16	420033.9	4417335	9.81	High	29.33	Low	0.00	Low	8.92	Very low
BH -17	420234	4417898	9.11	High	36.07	Moderate	0.64	Low	7.30	Very low
BH -18	420472.1	4418059	8.90	High	20.83	Low	4.07	Low	11.36	Very low
BH -19	420746.2	4418082	5.99	High	17.97	Low	0.00	Low	5.43	Very low
BH -20	420153	4416584	8.59	High	19.82	Low	0.00	Low	7.34	Very low
BH -21	420220	4416737	0.00	Low	11.93	Very low	0.00	Low	0.00	Very low
BH -22	419975.2	4416911	6.86	High	26.32	Low	1.20	Low	7.96	Very low
BH -23	420377.8	4416778	4.88	Low	7.55	Very low	0.00	Low	4.36	Very low
BH -24	420136	4416957	4.88	Low	12.16	Very low	0.00	Low	4.36	Very low
BH -25	420132.9	4417156	5.89	High	17.15	Low	0.00	Low	6.02	Very low
BH -26	420465.1	4417700	6.05	High	18.61	Low	0.00	Low	6.33	Very low
BH -27	420838.3	4417739	13.25	High	49.30	Moderate	0.64	Low	14.74	Very low
BH -28	420228	4417361	8.64	High	43.65	Moderate	0.64	Low	7.30	Very low
BH -29	420312	4418018	6.79	High	36.72	Moderate	0.00	Low	5.73	Very low
BH -30	420132	4417887	5.98	High	15.15	Low	0.00	Low	6.18	Very low
BH -31	420066	4417202	5.05	High	25.36	Low	0.00	Low	4.61	Very low
BH -32	419946.8	4417397	6.57	High	32.06	Low	0.00	Low	5.15	Very low
BH -33	419501.7	4417523	1.14	Low	15.06	Low	0.00	Low	0.00	Very low
BH -34	419426.9	4417387	0.00	Low	4.13	Very low	0.00	Low	0.00	Very low
BH -35	419142.7	4417518	0.00	Low	7.38	Very low	0.00	Low	0.00	Very low
BH -36	419463.7	4417598	0.00	Low	2.82	Very low	0.00	Low	0.00	Very low
BH -37	414438.1	4422272	0.24	Low	16.02	Low	0.00	Low	0.00	Very low
BH -38	414471.5	4422043	0.00	Low	12.56	Very low	0.00	Low	0.00	Very low
BH -39	414785.9	4422158	0.00	Low	11.60	Very low	0.00	Low	0.00	Very low
BH -40	414785.4	4422400	0.35	Low	9.76	Very low	0.00	Low	0.00	Very low
BH -41	415094	4423149	0.00	Low	3.11	Very low	0.00	Low	0.00	Very low
BH -42	414826.9	4423451	0.00	Low	4.41	Very low	0.00	Low	0.00	Very low
BH -43	414425.5	4423649	0.00	Low	9.52	Very low	0.00	Low	0.00	Very low
BH -44	414046.9	4423173	0.00	Low	4.77	Very low	0.00	Low	0.00	Very low
BH -45	414083	4423536	0.02	Low	9.95	Very low	0.00	Low	0.00	Very low
BH -46	413568.4	4423843	2.31	Low	17.28	Low	0.00	Low	1.42	Very low
BH -47	414611.8	4423512	0.00	Low	0.00	Very low	0.00	Low	0.00	Very low
BH -48	414491.5	4423519	0.00	Low	0.15	Very low	0.00	Low	0.00	Very low
BH -49	414801.9	4423327	0.00	Low	3.71	Very low	0.00	Low	0.00	Very low
BH -50	413855.6	4424058	0.00	Low	2.46	Very low	0.00	Low	0.00	Very low
BH -51	414073.3	4423864	0.00	Low	1.53	Very low	0.00	Low	0.00	Very low
BH -52	414281	4423344	0.00	Low	0.71	Very low	0.00	Low	0.00	Very low
BH -53	414364.6	4423695	0.00	Low	0.00	Very low	0.00	Low	0.00	Very low
BH -54	414587.7	4423714	0.00	Low	0.31	Very low	0.00	Low	0.00	Very low

BH -55	414598.8	4423922	0.00	Low	0.00	Very low	0.00	Low	0.00	Very low
BH -56	414899.2	4423194	0.00	Low	5.82	Very low	0.00	Low	0.00	Very low
BH -57	414605.1	4423086	0.00	Low	5.29	Very low	0.00	Low	0.00	Very low
BH -58	416304.5	424021.6	0.00	Low	1.13	Very low	0.00	Low	0.00	Very low
BH -59	416423.6	4423805	0.00	Low	5.00	Very low	0.00	Low	0.00	Very low
BH -60	416244.2	4423548	0.00	Low	1.66	Very low	0.00	Low	0.00	Very low
BH -61	416032.8	4423386	0.37	Low	5.11	Very low	0.00	Low	0.00	Very low
BH -62	416142	4423618	0.00	Low	3.91	Very low	0.00	Low	0.00	Very low
BH -63	416207.3	4423403	0.00	Low	3.64	Very low	0.00	Low	0.00	Very low
BH -64	416087.4	4423155	0.00	Low	6.66	Very low	0.00	Low	0.00	Very low
BH -65	415913.3	4423693	0.00	Low	12.00	Very low	0.00	Low	0.00	Very low
BH -66	416419.3	4423516	0.00	Low	1.55	Very low	0.00	Low	0.00	Very low
BH -67	416011.7	4423560	0.00	Low	3.53	Very low	0.00	Low	0.00	Very low
BH -68	416508	4423607	0.00	Low	0.00	Very low	0.00	Low	0.00	Very low
BH -69	419682.1	4417474	16.23	Very high	63.33	High	0.00	Low	10.19	Very low
BH -70	419719.9	4417094	28.98	Very high	75.00	High	1.50	Low	27.07	Low
BH -71	419767	4416291	20.26	Very high	74.01	High	2.36	Low	22.49	Low
BH -72	419333.3	4416396	29.43	Very high	63.54	Moderate	6.03	High	30.09	Low
BH -73	419191.7	4416756	25.10	Very high	77.03	High	1.22	Low	25.69	Low
BH -74	419450.2	4416972	37.97	Very high	86.03	Very high	4.95	Low	41.40	Moderate
BH -75	419324	4417227	30.25	Very high	68.28	High	8.31	High	32.54	Low
BH -76	418959.9	4416782	33.42	Very high	71.82	High	3.84	Low	33.89	Low
BH -77	418903.1	4417062	31.93	Very high	84.10	High	5.65	High	36.28	Moderate
BH -78	418661.5	4416847	27.34	Very high	70.38	High	2.56	Low	24.63	Low
BH -79	419105.6	4416342	23.92	Very high	72.44	High	6.16	High	25.90	Low
BH -80	418554.4	4417218	40.75	Very high	88.01	Very high	11.98	High	48.68	Moderate
BH -81	418567.4	4416515	27.59	Very high	78.56	High	3.21	Low	25.96	Low
BH -82	418124.3	4417014	33.12	Very high	82.24	High	4.18	Low	37.62	Moderate
BH -83	417962.2	4415532	21.49	Very high	74.68	High	2.34	Low	20.92	Low
BH -84	417531	4417914	17.78	Very high	51.66	Moderate	5.21	High	20.61	Low
BH -85	416822.7	4418631	31.58	Very high	81.63	High	7.05	High	35.14	moderate

7. Conclusions

This study deals with the liquefaction potentials of several districts, comprising Area_1, Area_2 and Area_3, in Iğdır city located in the eastern side of Türkiye. The city borders with three seismically active countries (i.e. Armenia, Nakhicivan and Iran) is located in a plain land and sits on Quaternary alluvial deposits, likewise the studied areas. Moreover, the site has been surrounded by several fault lines with potentially high magnitude earthquake triggering capabilities which may influence the city with as large as 0.393g and subsequently with 0.225g input motions. Due to these reasons, the study maps the liquefaction potential of the aforementioned areas within the city by considering soil data from 85 boreholes in total. The liquefaction potential is assessed at 0.393g and 0.225g seismic intensity levels with respect to two methods; (i) Liquefaction Potential Index (LPI) and (ii) Liquefaction Severity Index (L_s). The outcomes of the study can be listed as follows:

- Based on LPI and L_s criteria, the Area_1 located in the south-east side of the city is particularly prone to liquefaction as most part of the area is categorized by very high (LPI) and high (L_s) liquefaction probability under PGA of 0.393g.
- The Area_2 positioned on the north-west side of the city may also endure liquefaction effect with high to very high extents (LPI) or with low to high extents (L_s).

- Subsequently, in the south part of the city (Area_3), the liquefaction phenomena is expected to be recognized as very low by both LPI and L_s methods.
- As anticipated, when the city is hit by an input motion with PGA of 0.225g, liquefaction potential or severity stretch down to the lower categories. In particular, the Area_1 and the Area_3 are depicted to be non-liquefiable or very low liquefaction susceptibility. The Area_2 falls into, mostly, very low to low and, partially, high categories with respect to LPI criteria and low and very low (most proportion of the area) and moderate concerning L_s criteria.
- Finally, the studied areas at Igdir city are likely to persist liquefaction with varied degrees of severity. This study expresses the liquefaction potential at the city that may be benefitted for seismic risk mitigation, earthquake hazard assessments and urban planning policies.

Competing Interest

The authors declare that they do not have any competing interest.

Acknowledgement

The authors thanks to the Igdir Municipality for sharing the geotechnical data of the studied areas.

References

- [1] Kramer S. L. 1996. Geotechnical earthquake engineering. Pearson Education India
- [2] Cabalar A. F., Canbolat A., Akbulut N., Tercan S. H., Isik H. 2019. Soil liquefaction potential in Kahramanmaras, Türkiye. *Geomatics Natural Hazards and Risk*, 10(1), 1822-38. <https://doi.org/10.1080/19475705.2019.1629106>
- [3] Rouholamin M., Bhattacharya S., Orense R. P. 2017. Effect of initial relative density on the post-liquefaction behaviour of sand. *Soil Dynamics and Earthquake Engineering*, 97, 25-36. <https://doi.org/10.1016/j.soildyn.2017.02.007>
- [4] Yoshida N., Tokimatsu K., Yasuda S., Kokusho T., Okimura T. 2001. Geotechnical aspects of damage in Adapazari City during 1999 Kocaeli, Turkey earthquake. *Soils and Foundations*, 41(4), 25-45. https://doi.org/10.3208/sandf.41.4_25
- [5] Allen J., Bradley B., Green R., Orense R., Wotherspoon L., Ashford S., et al. 2010. Geotechnical reconnaissance of the 2010 Darfield (Canterbury) earthquake. *Bulletin of New Zealand Society for Earthquake Engineering*, 43(4), 243. <https://doi.org/10.5459/bnzsee.43.4.243-320>
- [6] Papathanassiou G., Mantovani A., Tarabusi G., Rapti D., Caputo R. 2015. Assessment of liquefaction potential for two liquefaction prone areas considering the May 20, 2012 Emilia (Italy) earthquake. *Journal of Environmental Earth Sciences*, 189, 1-16. <https://doi.org/10.1016/j.enggeo.2015.02.002>
- [7] Yasuda S. 2014. Allowable Settlement and Inclination of Houses Defined After the 2011 Tohoku: Pacific Ocean Earthquake in Japan. *Geotechnical Geological and Earthquake Engineering*, 28, 141-57. https://doi.org/10.1007/978-3-319-03182-8_5
- [8] Sassa S., Takagawa T. 2019. Liquefied gravity flow-induced tsunamis: first evidence and comparison from the 2018 Indonesia Sulawesi earthquake and tsunami disasters. *Landslides*, 16(1), 195-200. <https://doi.org/10.1007/s10346-018-1114-x>
- [9] Cakir, E., Cetin, K. O. 2024. Liquefaction triggering and induced ground deformations at a metallurgical facility in Dörtöyl-Hatay after the February 6 Kahramanmaraş earthquake sequence. *Soil Dynamics and Earthquake Engineering*, 178, 108465. <https://doi.org/10.1016/j.soildyn.2024.108465>
- [10] Ozener, P., Monkul, M. M., Bayat, E. E., Ari, A., Cetin, K. O. 2024. Liquefaction and performance of foundation systems in Iskenderun during 2023 Kahramanmaras-Turkiye earthquake sequence. *Soil Dynamics and Earthquake Engineering*, 178, 108433. <https://doi.org/10.1016/j.soildyn.2023.108433>
- [11] Yilmaz C., Silva V., Weatherill G. 2021. Probabilistic framework for regional loss assessment due to earthquake-induced liquefaction including epistemic uncertainty. *Soil Dynamics and Earthquake Engineering*, 141, 106493. <https://doi.org/10.1016/j.soildyn.2020.106493>
- [12] Zhang W., Lim K. W., Ghahari S. F., Arduino P., Tacioglu E. 2021. On the implementation and validation of a three-dimensional pressure-dependent bounding surface plasticity model for soil nonlinear wave propagation and soil-structure interaction analyses. *International Journal for Numerical and Analytical Methods in Geomechanics*, 45(8), 1091-119. <https://doi.org/10.1002/nag.3194>

- [13] Kiyota T., Koseki J., Sato T., Tsutsumi Y. 2009. Effects of sample disturbance on small strain characteristics and liquefaction properties of holocene and pleistocene sandy soils. *Soils and Foundations*, 49(4), 509-23. [https://doi.org/ 10.3208/sandf.49.509](https://doi.org/10.3208/sandf.49.509)
- [14] Kiyota T., Maekawa Y., Wu C. 2019. Using in-situ and laboratory-measured shear wave velocities to evaluate the influence of soil fabric on in-situ liquefaction resistance. *Soil Dynamics and Earthquake Engineering*, 117, 164-73. [https://doi.org/ 10.1016/j.soildyn.2018.11.016](https://doi.org/10.1016/j.soildyn.2018.11.016)
- [15] Lees J. J., Ballagh R. H., Orense R. P., van Ballegooy S. 2015. CPT-based analysis of liquefaction and re-liquefaction following the Canterbury earthquake sequence. *Soil Dynamics and Earthquake Engineering*, 79, 304-314. [https://doi.org/ 10.1016/j.soildyn.2015.02.004](https://doi.org/10.1016/j.soildyn.2015.02.004)
- [16] Facciorusso J., Madiati C., Vannucchi G. 2015. CPT-Based Liquefaction Case History from the 2012 Emilia Earthquake in Italy. *Journal of Geotechnical and Geoenvironmental Engineering*, 141(12). [https://doi.org/ 10.1061/\(asce\)gt.1943-5606.0001349](https://doi.org/10.1061/(asce)gt.1943-5606.0001349)
- [17] Chern S. G., Lee C. Y. 2009. CPT-based simplified liquefaction assessment by using fuzzy-neural network. *Journal of Marine Science and Technology-Taiwan*, 17(4), 326-31. [https://doi.org/ 10.51400/2709-6998.2024](https://doi.org/10.51400/2709-6998.2024)
- [18] Seed H. B., Idriss I. M. 1971. Simplified Procedure for Evaluating Soil Liquefaction Potential. *Journal of the Soil Mechanics and Foundation Division*, 97(SM9), 1249-73. [https://doi.org/ 10.1061/JSFEAQ.0001662](https://doi.org/10.1061/JSFEAQ.0001662)
- [19] Youd T. L., Idriss I. M., Andrus R. D., Arango I., Castro G., Chritrian J., et al. 2001. Liquefaction resistance of soils: summary report from the 1996 NCEER and 1998 NCEER/NSF workshops on evaluation of liquefaction resistance of soils. *Journal of Geotechnical and Geoenvironmental Engineering*, 127(10), 817-33. [https://doi.org/ 10.1061/\(ASCE\)1090-0241\(2001\)127:10\(817\)](https://doi.org/10.1061/(ASCE)1090-0241(2001)127:10(817))
- [20] Cetin K. O., Seed H. B., Der Kiureghian A., Tokimatsu K., Harder L., Kayen R., et al. 2004. SPT-Based probabilistic and deterministic assessment of seismic soil liquefaction potential. *Journal of Geotechnical and Geoenvironmental Engineering*, 130(12), 1314-40. [https://doi.org/ 10.1016/j.dib.2018.08.043](https://doi.org/10.1016/j.dib.2018.08.043)
- [21] Duman, E. S., Ikizler, S. B., & Angin, Z. E. K. A. I. (2015). Evaluation of soil liquefaction potential index based on SPT data in the Erzincan, Eastern Turkey. *Arabian Journal of Geosciences*, 8, 5269-5283. [https://doi.org/ 10.1007/s12517-014-1550-4](https://doi.org/10.1007/s12517-014-1550-4)
- [22] Yıldız, Ö. (2022). Seismic site characterization of Battalgazi in Malatya, Turkey. *Arabian Journal of Geosciences*, 15(9), 867. <https://doi.org/10.1007/s12517-022-10170-x>
- [23] Akkaya, İ., Özvan, A., Akin, M., Akin, M. K., & Övün, U. (2018). Comparison of SPT and V s-based liquefaction analyses: a case study in Erciş (Van, Turkey). *Acta Geophysica*, 66, 21-38. <https://doi.org/10.1007/s11600-017-0103-0>
- [24] Avagyan, A., Sosson, M., Sahakyan, L., Sheremet, Y., Vardanyan, S., Martirosyan, M., Muller, C., 2018. Tectonic Evolution of the Northern Margin of the Cenozoic Ararat Basin, Lesser Caucasus, Armenia. *J Petr. Geol.* 41(4):495-511. [https://doi.org/ 10.1111/jpg.12718](https://doi.org/10.1111/jpg.12718)
- [25] Türkiye İstatistik Kurumu İl ve ilçelere göre il/ilçe merkezi, belde/köy nüfusu ve yıllık nüfus artış hızı, [online] Available at: <https://data.tuik.gov.tr/Kategori/GetKategori?p=nufus-ve-demografi-109&dil=1> [Accessed: 17.05.2023]
- [26] Karaoğlu M., Erdel E. 2022. A Study of Soil and Land Features with Geographic Information Systems (GIS) Analysis: İğdir, Türkiye. *Türkiye Tarımsal Araştırmalar Dergisi*, 9(2), 198-208. [https://doi.org/ 10.19159/tutad.1076908](https://doi.org/10.19159/tutad.1076908)
- [27] Koç A., Koç C. 2018. An Assessment through relationship between air pollution and climatic parameters in City of İğdir. *Journal of Urban Cultures and Managements*, 11(1), 1-10.
- [28] Öztürk M., Altay V., Altundağ E., Gücel S. 2016. Halophytic plant diversity of unique habitats in Turkey: Salt mine caves of Çankırı and İğdir. *Halophytes for food security in dry lands*, Elsevier, 291-315.
- [29] Bulut F., Bohnhoff M., Eken T., Janssen C., Kilic T., Dresen G. 2012. The East Anatolian Fault Zone: Seismotectonic setting and spatiotemporal characteristics of seismicity based on precise earthquake locations. *Journal of Geophysics Research-Solid Earth*, 117. [https://doi.org/ 10.1029/2011jb008966](https://doi.org/10.1029/2011jb008966)
- [30] Yavasoglu H., Tari E., Tuysuz O., Cakir Z., Ergintav S. 2011. Determining and modeling tectonic movements along the central part of the North Anatolian Fault (Turkey) using geodetic measurements. *Journal of Geodynamics*, 51(5), 339-43. [https://doi.org/ 10.1016/j.jog.2010.07.003](https://doi.org/10.1016/j.jog.2010.07.003)
- [31] Ministry of Disaster and Emergency Management Presidency (AFAD). <http://www.deprem.gov.tr/en/event-catalogue> (accessed at 12 December 2023).
- [32] Emre Ö., Duman T. Y., Özalp S., Şaroğlu F., Olgun Ş., Elmacı H., et al. 2018. Active fault database of Turkey. *Bulletin of Earthquake Engineering*, 16(8), 3229-75. [https://doi.org/ 10.1007/s10518-016-0041-2](https://doi.org/10.1007/s10518-016-0041-2)
- [33] Karakhanian A. S., Trifonov V. G., Philip H., Avagyan A., Hessami K., Jamali F., et al. 2004. Active faulting and natural hazards in Armenia, eastern Turkey and northwestern Iran. *Tectonophysics*, 380(3-4), 189-219. [https://doi.org/ 10.1016/j.tecto.2003.09.020](https://doi.org/10.1016/j.tecto.2003.09.020)
- [34] Wells D. L., Coppersmith K. J. 1994. New empirical relationships among magnitude, rupture length, rupture width, rupture area, and surface displacement. *Bulletin of the Seismological Society of America*, 84(4), 974-1002. [https://doi.org/ 10.1785/BSSA0840040974](https://doi.org/10.1785/BSSA0840040974)

- [35] Ulusay R., Tuncay E., Sonmez H., Gokceoglu C. 2004. An attenuation relationship based on Turkish strong motion data and iso-acceleration map of Turkey. *Engineering Geology*, 74(3-4), 265-91. <https://doi.org/10.1016/j.enggeo.2004.04.002>
- [36] Guzel, Y. 2024. Correlating Measured SPT-N, Shear Wave Velocity and Liquid Limit Values in Melekli Region, Igdir (Türkiye). *Journal of Advanced Research in Natural and Applied Sciences*, 10(1), 161-174. <https://doi.org/10.28979/jarnas.1393352>
- [37] Seed H. B., Idriss I. M. 1971. Simplified procedure for evaluating soil liquefaction potential. *Journal of the Soil Mechanics and Foundation Division*, 97(9), 1249-73.
- [38] Seed H. B., Tokimatsu K., Harder L. F., Chung R. M. 1985. Influence of spt procedures in soil liquefaction resistance evaluations. *Journal of Geotechnical Engineering-ASCE*, 111(12), 1425-45.
- [39] Liao S. S. C., Whitman R. V. 1986. Overburden correction factors for spt in sand. *Journal of Geotechnical Engineering-ASCE*, 112(3), 373-7. [https://doi.org/10.1061/\(asce\)0733-9410\(1986\)112:3\(373\)](https://doi.org/10.1061/(asce)0733-9410(1986)112:3(373))
- [40] Akin M. K., Kramer S. L., Topal T. 2016. Dynamic soil characterization and site response estimation for Erbaa, Tokat (Turkey). *Natural Hazards*, 82(3), 1833-68. <https://doi.org/10.1007/s11069-016-2274-4>
- [41] Seed R. B., Cetin K. O., Moss R. E., Kammerer A. M., Wu J., Pestana J. M., et al. 2003. Recent advances in soil liquefaction engineering: a unified and consistent framework. *Proceedings of the 26th Annual ASCE Los Angeles Geotechnical Spring Seminar: Long Beach, CA*.
- [42] Sonmez H. 2003. Modification of the liquefaction potential index and liquefaction susceptibility mapping for a liquefaction-prone area (Inegol,Turkey). *Environmental Geology*, 44(7), 862-71. <https://doi.org/10.1007/s00254-003-0831-0>
- [43] Tosun H., Ulusay R. 1997. Engineering geological characterization and evaluation of liquefaction susceptibility of foundation soils at a dam site, southwest Turkey. *Environmental and Engineering Geosciences*, 3(3), 389-409. <https://doi.org/10.2113/gsegeosci.III.3.389>
- [44] Ulusay R., Kuru T. 2004. 1998 Adana-Ceyhan (Turkey) earthquake and a preliminary microzonation based on liquefaction potential for Ceyhan town. *Natural Hazards*, 32(1), 59-88. <https://doi.org/10.1023/b:Nhaz.0000026790.71304.32>
- [45] Duman E. S., Ikizler S. B., Angin Z. 2015. Evaluation of soil liquefaction potential index based on SPT data in the Erzincan, Eastern Turkey. *Arabian Journal of Geosciences*, 8(7), 5269-83. <https://doi.org/10.1007/s12517-014-1550-4>
- [46] Seed H. B., Idriss I. 1982. *Ground motion and soil liquefaction during earthquakes*. Earthquake Engineering Research Institute, Berkeley, California.
- [47] Iwasaki T., Tokida K., Tatsuoka F., Watanabe S., Yasuda S., Sato H. 1981. Microzonation for soil liquefaction potential using simplified methods. *Proceedings of the 3rd international conference on microzonation, Seattle*, pp. 1310-30.
- [48] Sonmez H., Gokceoglu C. 2005. A liquefaction severity index suggested for engineering practice. *Environmental Geology*, 48(1), 81-91. <https://doi.org/10.1007/s00254-005-1263-9>